Human CD34$^+$ cells engineered to express membrane-bound tumor necrosis factor–related apoptosis-inducing ligand target both tumor cells and tumor vasculature

Cristiana Lavazza,[1,2] Carmelo Carlo-Stella,[1,2] Arianna Giacomini,[1,2] Loredana Cleris,[3] Marco Righi,[4] Daniela Sia,[1,2] Massimo Di Nicola,[1] Michele Magni,[1] Paolo Longoni,[1] Marco Milanesi,[1] Maura Francolini,[5] Annunziata Gloghini,[6] Antonino Carbone,[6] Franca Formelli,[3] and Alessandro M. Gianni[1,2]

[1]Medical Oncology, Fondazione Istituto di Ricovero e Cura a Carattere Scientifico, Istituto Nazionale Tumori, Milano; [2]Medical Oncology, Università degli Studi di Milano, Milano; [3]Experimental Oncology, Fondazione Istituto di Ricovero e Cura a Carattere Scientifico Istituto Nazionale Tumori, Milano; [4]Consiglio Nazionale delle Ricerche, Institute of Neuroscience, Milano; [5]Medical Pharmacology, Università degli Studi di Milano, Milano; and [6]Pathology, Fondazione Istituto di Ricovero e Cura a Carattere Scientifico Istituto Nazionale Tumori, Milano, Italy

Adenovirus-transduced CD34$^+$ cells expressing membrane-bound tumor necrosis factor–related apoptosis-inducing ligand (CD34-TRAIL$^+$ cells) exert potent antitumor activity. To further investigate the mechanism(s) of action of CD34-TRAIL$^+$ cells, we analyzed their homing properties as well as antitumor and antivascular effects using a subcutaneous myeloma model in immunodeficient mice. After intravenous injection, transduced cells homed in the tumor peaking at 48 hours when 188 plus or minus 25 CD45$^+$ cells per 10^5 tumor cells were detected. Inhibition experiments showed that tumor homing of CD34-TRAIL$^+$ cells was largely mediated by vascular cell adhesion molecule-1 and stromal cell–derived factor-1. Both CD34-TRAIL$^+$ cells and soluble (s)TRAIL significantly reduced tumor volume by 40% and 29%, respectively. Computer-aided analysis of TdT-mediated dUTP nick end-labeling–stained tumor sections demonstrated significantly greater effectiveness for CD34-TRAIL$^+$ cells in increasing tumor cell apoptosis and necrosis over sTRAIL. Proteome array analysis indicated that CD34-TRAIL$^+$ cells and sTRAIL activate similar apoptotic machinery. In vivo staining of tumor vasculature with sulfosuccinimidyl-6-(biotinamido) hexanoate-biotin revealed that CD34-TRAIL$^+$ cells but not sTRAIL significantly damaged tumor vasculature, as shown by TdT-mediated dUTP nick end-labeling$^+$ endothelial cells, appearance of hemorrhagic areas, and marked reduction of endothelial area. These results demonstrate that tumor homing of CD34-TRAIL$^+$ cells induces early vascular disruption, resulting in hemorrhagic necrosis and tumor destruction. (Blood. 2010;115:2231-2240)

Introduction

Genetically modified stem/progenitor cells represent an innovative approach for delivery of anticancer molecules.[1,2] Because of their homing properties, systemically injected stem/progenitor cells could infiltrate both primary and metastatic tumor sites, thus allowing tumor-specific targeting[3-9] and potentially overcoming limitations inherent to the pharmacokinetic profile of soluble drugs.[10-12]

Soluble tumor necrosis factor (TNF)–related apoptosis-inducing ligand (sTRAIL) is a proapoptotic member of the TNF superfamily of death receptor ligands. A variety of preclinical data show that sTRAIL is a cancer cell–specific molecule exerting a remarkable antitumor activity in vitro[13-18] and in vivo in athymic nude mice or in nonobese diabetic/severe combined immunodeficient (NOD/SCID) mice.[13,19,20] Phase 1/2 clinical trials have demonstrated a good toxicity profile for sTRAIL but limited evidence of antitumor activity probably because of short exposure of tumor cells to low drug concentrations.[21] Because of sTRAIL's short half-life,[13,20,22] it seems unlikely that the recommended sTRAIL dose of 8 mg/kg body weight will allow prolonged exposure of tumor cells at high drug concentrations.[21]

Strategies to enhance the therapeutic activity of sTRAIL include combining it with conventional chemotherapy[23] or with new agents, such as histone deacetylase inhibitors that up-regulate TRAIL-R1 and/or TRAIL-R2, resulting in a synergistic induction of apoptosis in both sTRAIL-sensitive and -resistant tumor cells.[24] Alternatively, cell-based vehiculation of the full-length, membrane-bound (m)TRAIL has been proposed.[11] Neural or mesenchymal stem cell–mediated mTRAIL delivery has been investigated in solid tumors.[9,25-28] More recently, we demonstrated that intravenous injection of mTRAIL-expressing CD34$^+$ cells (CD34-TRAIL$^+$ cells) efficiently act as mTRAIL-presenting vehicles and exert a potent antitumor activity in NOD/SCID mice bearing systemic multiple myeloma and non-Hodgkin lymphoma xenografts.[29-31]

Using a subcutaneous multiple myeloma model in NOD/SCID mice, the present study aimed at investigating the antitumor mechanism(s) of mTRAIL-expressing cells by analyzing homing properties of CD34-TRAIL$^+$ cells as well as the degree and distribution of tumor cell death and tumor vascular damage. To analyze the antivascular activity of CD34-TRAIL$^+$ cells, we used an in vivo staining assay of tumor vasculature.[32] The imaging software ImageJ (National Institutes of Health), equipped with appropriately designed macros to specifically quantify parameters of tumor cell and tumor vascular damage, allowed the processing

Submitted August 20, 2009; accepted December 17, 2009. Prepublished online as *Blood* First Edition paper, January 14, 2010; DOI 10.1182/blood-2009-08-239632.

The online version of this article contains a data supplement.

The publication costs of this article were defrayed in part by page charge payment. Therefore, and solely to indicate this fact, this article is hereby marked "advertisement" in accordance with 18 USC section 1734.

of whole histologic sections rather than manually selected images. Our data demonstrate that mTRAIL induces significant levels of tumor cell death by targeting both tumor cells and tumor vasculature, thus acting as a vascular-disrupting agent.

Methods

Reagents

Recombinant sTRAIL (KillerTRAIL) was purchased from Alexis Corporation and BoosterExpress reagent from Gene Therapy Systems. AMD3100[33] was obtained from Sigma-Aldrich.

Cell line and CD34$^+$ cells

The multiple myeloma cell line KMS-11 was cultured in RPMI 1640 supplemented with 10% fetal bovine serum and periodically tested for mycoplasma contamination. CD34$^+$ cells were positively selected using the AutoMACS device (Miltenyi Biotec) from the blood of consenting donors undergoing stem cell mobilization.

Adenoviruses

The cDNA for human TRAIL was purchased from the Riken BioResource Center.[34] A replication-deficient adenovirus encoding the human TRAIL gene (Ad-TRAIL) expressed from the CMV promoter was generated using standard methods. Briefly, the entire coding sequence of human TRAIL was cloned into the *Xho*I and *Not*I sites of pAd5CMVK-NpA. The resultant plasmid and adenovirus backbone sequences (Ad5) that had the E1 (E1A and E1B) genes deleted were transfected into human embryonic kidney 293 cells, and viral particles were isolated and amplified for analysis of TRAIL expression. Ad-TRAIL was screened for replication-competent virus using the A549 plaque assay, and the virus titer was determined by tissue culture infectious dose 50 on human embryonic kidney 293 cells. Purified virus was stored at −80°C in phosphate-buffered saline (PBS) with 3% sucrose until use. An adenovirus empty cassette (Ad-mock) used as control was purchased from the Center for Cell and Gene Therapy (Baylor College of Medicine).

Adenoviral transduction of CD34$^+$ cells

The transduction protocol has been described in detail elsewhere.[35] Briefly, CD34$^+$ cells were plated at 2×10^6/mL in 35-mm Petri dishes in 1 mL of serum-free Iscove modified Dulbecco medium containing an appropriate dilution of adenovector stock, allowing a final multiplicity of infection of 200 plaque-forming units/cell. After a 2-hour incubation (37°C, 5% CO_2), cultures were supplemented with 1 mL of Iscove modified Dulbecco medium/fetal bovine serum 20%, containing BoosterExpress reagent (final dilution 1:200) and further incubated for 18 hours. Mean transduction efficiency by flow cytometry was 90% plus or minus 3% (SEM).[29,35]

In vivo activity of CD34-TRAIL$^+$ cells in NOD/SCID mice

Six- to 8-week-old female NOD/SCID mice with body weight of 20 to 25 g were purchased from Charles River. Mice were housed under standard laboratory conditions according to our institutional guidelines. Animal experiments were performed according to the Italian laws (D.L. 116/92 and after additions), which enforce the EU 86/109 Directive and were approved by the institutional Ethical Committee for Animal Experimentation of Fondazione Istituti di Ricovero e Cura a Carattere Scientifico Istituto Nazionale Tumori. KMS-11 cells (5×10^6 cells/mouse) were inoculated subcutaneously in the left flank of each mouse. When tumor reached approximately 7 to 10 mm in diameter (usually 10-12 days after tumor inoculation), mice were randomly grouped to receive single or repeated treatments. Single treatments consisted of one intravenous injection of either CD34-TRAIL$^+$ cells (3×10^6 cells/mouse), mock-transduced CD34$^+$ cells (3×10^6 cells/mouse), or one intraperitoneal injection of sTRAIL (500 μg/mouse). After 48 to 72 hours, tumor nodules were excised and processed for histologic analysis. To inhibit intratumor homing of CD34-TRAIL$^+$ cells, mice received either one single intraperitoneal dose of anti–vascular cell adhesion molecule-1 (VCAM-1) antibody (clone M/K-2; Southern Biotechnology) at 0.5 mg/mouse, 3 hours before cell administration, or 2 doses of AMD3100 (5 mg/kg subcutaneously, 1 hour before and 3 hours after cell administration).[33] Repeated treatments consisted of daily injections of either CD34-TRAIL$^+$ cells or mock-transduced CD34$^+$ cells (1×10^6 cells/mouse/injection per day intravenously, days 12-15), or a 4-day course of recombinant sTRAIL (30 mg/kg per day intraperitoneally, days 12-15). Mice were checked twice weekly for tumor appearance, tumor dimensions, body weight, and toxicity. Tumor volumes were measured with calipers and their weights calculated using the formula: $(a \times b^2)/2$, where a and b represented the longest and shortest diameters, respectively. Mice were followed up for 3 weeks after the end of the treatments. The endpoint of the subcutaneous model was tumor weight. Each experiment was performed on at least 2 separate occasions, using 5 mice per treatment group.

In vivo biotinylation of tumor vasculature

To analyze tumor vasculature, proteins expressed on the luminal surface of vascular endothelium were in vivo biotinylated by intravenous injection of sulfosuccinimidyl-6-(biotinamido) hexanoate (sulfo-NHS-LC-biotin; Thermo Fisher Scientific). This compound is impaired in diffusion through biologic membranes and efficiently allows for the in vivo biotinylation of luminal vascular endothelial proteins.[32] Briefly, animals receiving CD34-TRAIL$^+$ cells, mock-transduced CD34$^+$ cells, or sTRAIL were intravenously injected with 0.2 mL of sulfo-NHS-LC-biotin (5 mg/mL) in polygeline. After 5 minutes, mice were intravenously injected with 1 mL of Tris/polygeline (50mM) to neutralize the circulating reagent. Tumors were then excised, embedded in cryoembedding compound, and freshly snap-frozen in isopentane precooled in liquid nitrogen for preparation of cryosections. Tumor endothelial cells were revealed by staining with horseradish peroxidase (HRP; Dako Denmark) or AlexaFluor 488– or 568–conjugated streptavidin (Invitrogen).

Histologic analysis and immunohistochemistry

Formalin-fixed, paraffin-embedded tumor nodules or healthy tissues (femur, lung, liver, and spleen) were stained with hematoxylin and eosin or processed for immunohistochemistry with mouse anti–human CD45 monoclonal antibody (Dako Denmark), mouse anti–mouse CD31 antibody (Santa Cruz Biotechnology), or rat anti–mouse glycophorin A (clone TER-119; BD Biosciences PharMingen). Apoptosis and tumor necrosis were detected using TdT-mediated dUTP nick end-labeling (TUNEL) staining (Roche Diagnostics) according to the manufacturer's instructions. Positive signal was revealed by 3,3′-diaminibenzidine staining, and tumor sections were then counterstained before analysis by light microscopy. Cryosections of in vivo biotinylated tumor nodules (thickness of 4 μm) were dried on positively charged glass slides. Sections were fixed with cold acetone (5 minutes at 4°C), rinsed with PBS, and then immersed in 0.03% hydrogen peroxide to block endogenous peroxidase. Sections were then rinsed with PBS containing 0.05% Tween 20, blocked for 10 minutes with 2% bovine serum albumin, and incubated with 1 μg/mL HRP-conjugated streptavidin diluted in PBS (1 hour, room temperature). Biotinylated tumor endothelium was revealed by 3,3′-diaminobenzidine staining. Sections were examined under a light microscope (BX51; Olympus) and acquired with an automatic high-resolution scanner (dotSlide System; Olympus). Image processing was carried out using dotSlide software (Olympus).

Immunofluorescence and confocal microscopy

Cryosections were fixed with acetone (5 minutes, 4°C), rinsed with PBS, and then blocked with 2% bovine serum albumin. Sections were first incubated with the appropriate primary antibody, including mouse anti–human leukocyte common antigen CD45 (Dako North America), mouse anti–human stromal cell–derived factor-1 (SDF-1; R&D Systems), rat anti–mouse VCAM-1 (Southern Biotechnology), or hamster anti–mouse TRAIL-R2 (BD Biosciences PharMingen). After washing, sections were

incubated with the appropriate AlexaFluor 568–conjugated secondary antibody (Invitrogen). Biotinylated tumor vessels were revealed with AlexaFluor 488–conjugated streptavidin (Invitrogen). To detect apoptotic endothelial cells, cryosections from in vivo biotinylated tumors were double stained with TUNEL (Roche Diagnostics) and AlexaFluor 568–conjugated streptavidin (Invitrogen) and finally incubated with TO-PRO-3 nuclear dye (Invitrogen). Sections were examined under an epifluorescent microscope equipped with a laser confocal system (MRC-1024; Bio-Rad). Image processing was carried out using LaserSharp computer software (Bio-Rad).

Analysis of stained sections

After appropriate staining, images of tissue sections were acquired at ×20 magnification with an automatic high-resolution scanner (dotSlide System; Olympus) and subdivided into a collection of nonoverlapping red, green, and blue (RGB) images in TIFF format (final resolution 3.125 pixels/μm). For necrosis quantification, images were acquired at ×2 magnification without further subdivision. Image analysis was carried out using the open-source ImageJ software (http://rsb.info.nih.gov/ij/). Routines for image analysis were coded in ImageJ macro language and executed on RGB images without further treatment. Per each experimental condition, at least 3 sections from different tumor nodules or healthy tissues were analyzed. Intratumor frequency of CD34-TRAIL$^+$ cells was expressed as the number of CD45$^+$ cells per 10^5 total cells. Total cells were counted by the ImageJ internal function for particle analysis, whereas CD45$^+$ cells were manually counted in all images from whole scanning of histochemically stained tissue sections.

The number of total and TUNEL$^+$ cells per section was counted as follows. Briefly, the dynamic range of images was expanded to full by contrast enhancement, and cells were identified by appropriate filtering in the RGB channels. Resulting black-and-white images were combined to represent only pixels selected in every color channel. For each image, both total and TUNEL$^+$ cells were counted by the ImageJ internal function for particle analysis. TUNEL-stained sections were also analyzed for the presence of necrotic areas. Images were at first treated for noise reduction by application of a median filter with a 1.5-pixel radius. Then necrotic and total tissue areas were recognized using different filter values under direct human supervision. Black areas in the final binary images were quantified in terms of pixel counts to obtain a percentage necrotic index expressed as (necrotic area)/(total tissue area) × 100.

Tumor vasculature was analyzed on cryosections from in vivo biotinylated mice stained with HRP-conjugated streptavidin. To calculate endothelial area, ie, the percentage of tissue section occupied by endothelium, endothelial cells were identified by contrast enhancement and appropriate filtering. Background signal was removed considering only structures larger than an arbitrary minimal value. To analyze vessel wall thickness, we manually selected rectangular regions of RGB input images containing at least a hollow vessel. An automatic routine computed vessel thickness according to the formula: thickness = 2 × (vessel area)/[(vessel perimeter) + (lumen perimeter)]. At first, endothelial tissue was identified applying a threshold on the blue channel and obtaining a binary image representative of its distribution. Then, the lumen of each vessel in the image was identified as a nonendothelial area, ringed by endothelial tissue and greater than an arbitrary threshold. This procedure rejected smaller artifacts and allowed for recognition of hollow vessels, even when erythrocytes or other cells occupied the lumen. Subsequently, we identified the endothelium surrounding a given lumen by an iterative procedure. At first, we subdivided the binary representation of stained tissue into areas by a watershed algorithm. Then we selected only those regions adjacent to the lumen, obtaining a minimal image of the vessel wall. This minimal image was used to compute a working thickness according to the previously stated formula. Then, to avoid arbitrary removal of bona fide portions of the walls, we calculated a theoretical vessel contour expanding the lumen outline by several pixels equivalent to the working thickness. We next turned back to the watershedded image of endothelium distribution, selecting only those areas connected with the new, theoretical contour. Inclusion of the new regions in the minimal image produced the final vessel image. Both images were saved to allow for manual appreciation of proper vessel identification. At last, the final vessel thickness was calculated after assessment of the final vessel area and external perimeter. Per each parameter, the accuracy and appropriate cut-off levels were determined by comparing processed images to the RGB originals. In all instances, automatic routines were validated by comparing results with those obtained by visual counting of up to 10% of the total images by 2 independent pathologists.

Protein extraction and proteome profiler array

A total of 4 tissue sections, 30-μm thick, were cut from freshly snap-frozen nodules and homogenized in lysis buffer (1% NP-40, 20mM Tris-HCl pH 8.0, 137mM NaCl, 10% glycerol, 2mM ethylenediaminetetraacetic acid, 1mM orthovanadate, 10 μg/mL aprotinin, 10 μg/mL leupeptin in water) for 3 hours, on a rocking platform shaker at 2°C to 8°C. After vortexing, supernatants were collected by centrifugation (14 000 rpm, 30 minutes, 4°C) and then stored at −80°C or quantified using the Bio-Rad protein assay (Bio-Rad). The Proteome Profiler Human Apoptosis array kit (R&D Systems) was performed according to the manufacturer's instructions. Briefly, equal amounts of proteins (500 μg) from control and treated mice were diluted and incubated with the apoptosis array overnight at 4°C. After washing of unbound material, a cocktail of apoptosis-detection HRP-conjugated antibodies was used to reveal apoptosis-related proteins by chemiluminescence. Array images on developed X-ray film (GE Healthcare) were scanned and finally analyzed following the manufacturer's indications using ImageJ. Results of array analysis were confirmed by Western blots.[29]

Statistical analysis

Statistical analysis was performed with the statistical package Prism 5 (GraphPad Software) run on a Macintosh Pro personal computer (Apple Computer). To test the probability of significant differences between untreated and treated samples, the Student *t* test for paired or unpaired data (2-tailed) was used. Tumor volume data were statistically analyzed with 2-way analysis of variance, and individual group comparisons were evaluated by Bonferroni post test. TUNEL staining and tumor vasculature data were statistically analyzed with 1-way analysis of variance, and individual group comparisons were evaluated by Bonferroni multiple comparison test. Differences were considered significant if P is less than or equal to .05.

Results

Antitumor effects of CD34-TRAIL$^+$ cells

To investigate the antitumor activity of CD34-TRAIL$^+$ cells, subcutaneous tumor-bearing NOD/SCID mice received 4 daily intravenous injections of transduced cells. Treatment was started when tumors reached approximately 7 to 10 mm in diameter. Compared with controls, both CD34-TRAIL$^+$ cells and sTRAIL significantly inhibited tumor growth by day 28, when tumor volumes were reduced by 38% ($P < .05$) and 31% ($P < .05$), respectively. On day 35, CD34-TRAIL$^+$ cells induced a 40% reduction in tumor growth over controls (4.2 ± 1.2 g vs 7.0 ± 2.0 g, $P < .001$), whereas a 29% reduction of tumor growth was detected in mice receiving sTRAIL (5.0 ± 1.7 g vs 7.0 ± 2.0 g, $P < .001$; Figure 1).

Vascular signals mediate tumor homing of CD34-TRAIL$^+$ cells

In vivo distribution of transduced cells was investigated in tumor-bearing NOD/SCID mice who received a single intravenous injection of CD34-TRAIL$^+$ cells (3×10^6 cells/mouse). Tumor and healthy tissue sections were immunostained with an anti–human CD45 antibody and digitally recorded to count transduced cells on entire tissue sections. Low frequencies of transduced cells were detected within tumors as early as 30 minutes after injection.

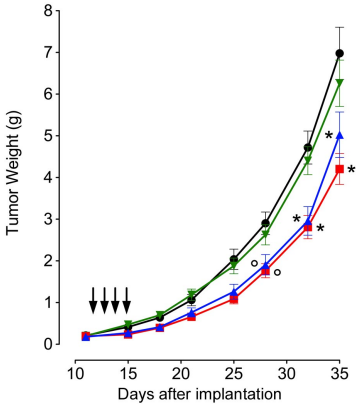

Figure 1. Effect of CD34-TRAIL$^+$ cells on KMS-11 tumor growth. NOD/SCID mice bearing SC tumor nodules 10 mm in diameter were randomly assigned to the different treatment groups, including daily injections of CD34-TRAIL$^+$ cells (red square) or mock-transduced CD34$^+$ cells (green inverted triangle; 1×10^6 cells/mouse/injection per day intravenously, days 12-15), a 4-day course of recombinant sTRAIL (blue triangle; 30 mg/kg per day intraperitoneally, days 12-15), and control vehicle (●). Arrows indicate treatment administration. Mean (± SEM) tumor weight data are shown. °$P < .05$, *$P < .001$ compared with controls.

They progressively increased and peaked 48 hours after injection when on average 188 plus or minus 25 CD45$^+$ cells per 10^5 tumor cells (ie, 0.2% ± 0.03%) were recorded (Figure 2). Confocal microscopy analysis revealed that injected CD34-TRAIL$^+$ cells were preferentially located close to the vessel wall, as detected by streptavidin–Alexa 488 and anti-CD45 Alexa 568 double-staining of in vivo biotinylated tumors (Figure 3A).

Early after injection, transduced cells were detected at high frequencies in the lung, liver, and spleen (Figure 2). CD34-TRAIL$^+$ cells progressively decreased and were no longer detectable in these tissues 24 hours after injection. Bone marrow CD34-TRAIL$^+$ cells peaked 5 hours after injection and were detectable up to 24 hours. Overall, kinetics data show that transduced cells transiently circulate through healthy tissues, whereas they are preferentially recruited within tumor nodules, allowing the hypothesis that homing signals by tumor endothelial cells actively promote intratumor homing of transduced cells.

Indeed, 30% of tumor vessels expressed high levels of VCAM-1 on the luminal surface (Figure 3Cii-iii),[4] whereas SDF-1 was ubiquitously expressed on tumor vessels and tumor cells (Figure 3Cv-vi; supplemental Figure 1, available on the *Blood* website; see the Supplemental Materials link at the top of the online article), suggesting a critical role of α4β1 integrins[35] and the CXCR4 chemokine[36,37] in regulating intratumor homing of mTRAIL-expressing cells. The functional relevance of SDF-1/CXCR4 and VCAM-1/VLA-4 pathways was supported by a significantly reduced tumor homing of CD34-TRAIL$^+$ cells in mice administered with anti–VCAM-1 antibody (0.09% ± 0.01%, $P = .001$) or the CXCR4 antagonist AMD3100[38] (0.05% ± 0.006%, $P < .001$), compared with controls (0.2% ± 0.03%, Figure 3B). The combination of AMD3100 and anti–VCAM-1 antibody failed to further reduce homing of transduced cells, probably because of ubiquitous expression of CXCR4 on CD34-TRAIL$^+$ cells and SDF-1 on tumor endothelial cells. In addition, approximately 8% to 12% of tumor endothelial cells expressed TRAIL-R2 receptor on their luminal surface (Figure 3Cviii-ix), suggesting that mechanisms other than SDF-1/CXCR4 and VCAM-1/VLA-4, such as the mTRAIL/TRAIL-R2 interactions, might be involved in regulating intratumor homing of CD34-TRAIL$^+$ cells.

CD34-TRAIL$^+$ cells induce tumor cell apoptosis

Consistent with the tumor-homing capacity of transduced cells, TUNEL staining revealed that CD34-TRAIL$^+$ cells effectively induced apoptosis of tumor cells.[29] To obtain an objective quantification of apoptosis, a computer-aided image analysis using ImageJ software was performed. Compared with controls, TUNEL$^+$ cells were increased by 8-fold (2.4% ± 1.4% vs 0.3% ± 0.3%, $P < .001$) and 4-fold (1.2% ± 0.7% vs 0.3% ± 0.3%, $P < .001$) after treatment with CD34-TRAIL$^+$ cells and sTRAIL, respectively (Figure 4B). Indeed, apoptotic effects of CD34-TRAIL$^+$ cells were significantly more potent than those exerted by sTRAIL ($P < .001$). To investigate whether mTRAIL-triggered tumor cell death involved the same signaling pathway as sTRAIL,[21] we profiled apoptotic proteins. As shown in Figure 4C, CD34-TRAIL$^+$ cells and sTRAIL activated similar apoptotic mediators, belonging to either extrinsic

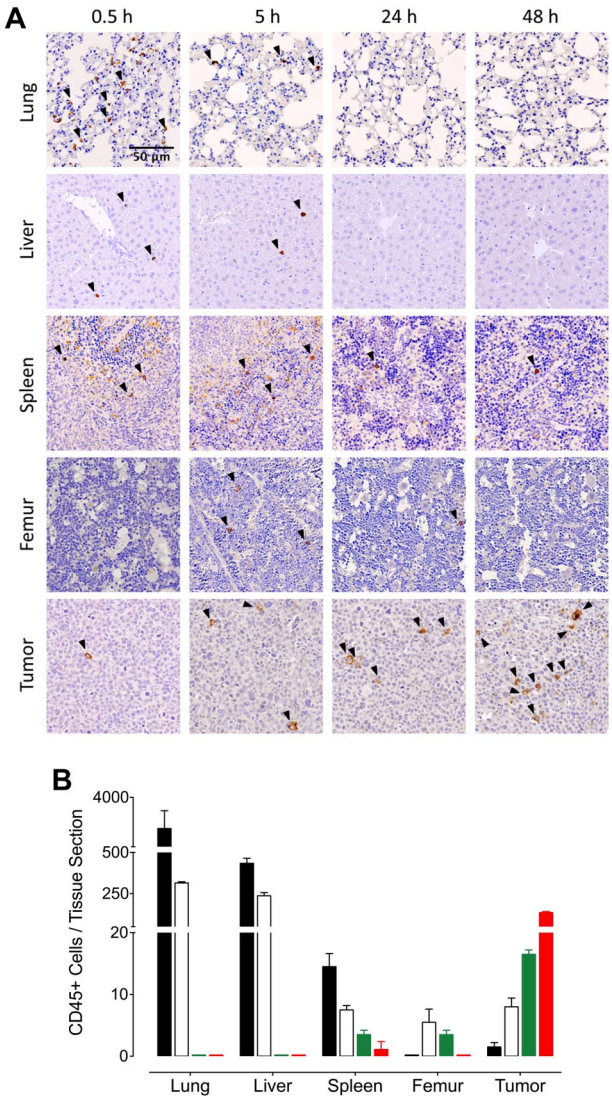

Figure 2. Tissue kinetics of CD34-TRAIL$^+$ cells. Lung, liver, spleen, femur, and tumor were harvested from tumor-bearing NOD/SCID mice 0.5 (■), 5 (□), 24 (green bars), and 48 (red bars) hours after a single intravenous injection of CD34-TRAIL$^+$ cells (3×10^6 cells/mouse). (A) Immunohistochemical staining with anti-CD45 antibody was used to detect CD34-TRAIL$^+$ cells (arrowheads). Representative images are shown. Objective lens, original magnification: 0.75 NA dry objective, 20×. (B) Quantification of CD34-TRAIL$^+$ cells on digitally acquired tissue sections stained with anti-CD45. Mean (± SD) number of CD45$^+$ cells per tissue section are shown. At least 3 sections from different animals were analyzed per each tissue.

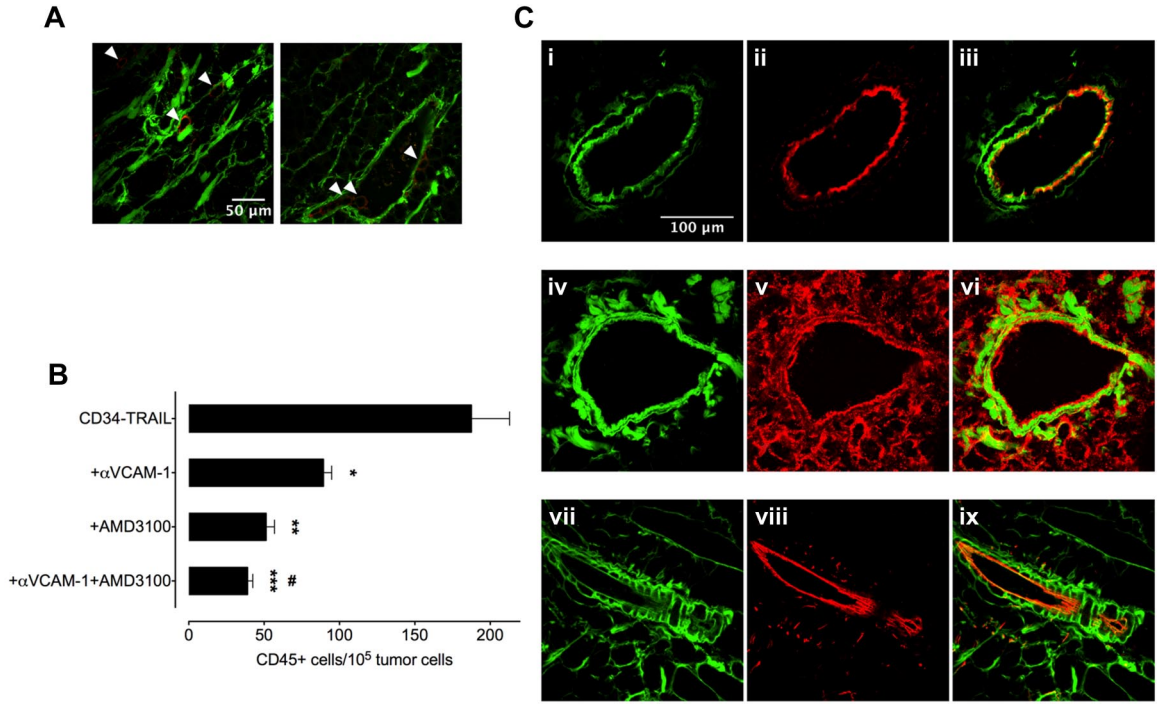

Figure 3. Intratumor homing of CD34-TRAIL+ cells involves SDF-1 and VCAM-1. (A) Forty-eight hours after a single intravenous injection of CD34-TRAIL+ cells, NOD/SCID mice were intravenously injected with 0.2 mL of sulfo-NHS-LC-biotin to biotinylate tumor vasculature. AlexaFluor 488–conjugated streptavidin and Alexa 568–conjugated anti-CD45 double staining of cryosections was used to detect tumor vessels (green) and CD34-TRAIL+ cells (red), respectively. CD34-TRAIL+ cells (arrowheads) infiltrating tumor tissue were found within tumor tissue near blood vessels. Objective lens, original magnification: 1.0 NA oil objective, 40×. (B) Forty-eight hours after a single intravenous injection of CD34-TRAIL+ cells (3×10^6 cells/mouse) alone or in combination with anti–VCAM-1 and/or AMD3100, tumor sections were immunohistochemically stained with anti-CD45 monoclonal antibody. Mean (± SD) number of CD34-TRAIL+ cells that had homed to tumors was determined by counting CD45+ cells per 10^5 tumor cells. Results of 1 representative experiment are shown. *$P = .001$, compared with controls. **$P < .001$, compared with controls. ***$P < .001$, compared with controls. #$P < .001$, compared with anti–VCAM-1. (C) Analysis of intratumor recruiting signals was carried out on 4-μm cryosections from in vivo biotinylated tumors. Cryosections were stained with AlexaFluor 488–conjugated streptavidin (green) to detect tumor vasculature (i,iv,vii). Cryosections were also stained with anti–VCAM-1 (ii), anti–SDF-1 (v), or anti–TRAIL-R2 (viii) followed by the appropriate AlexaFluor 568–conjugated secondary antibody for indirect detection of the corresponding antigen (red). Merged images demonstrate VCAM-1 (iii), SDF-1 (vi), or TRAIL-R2 (ix) expression by endothelial cells. Objective lens, original magnification: 1.0 NA oil objective, 40×.

(TRAIL-R1, TRAIL-R2, and FADD) or intrinsic pathways (Bcl-2 family members, mitochondrial mediators), resulting in a functionally effective release of a caspase-3–cleaved fragment.

CD34-TRAIL+ cells induce hemorrhagic necrosis

Tumor nodules excised from mice receiving CD34-TRAIL+ cells had a soft consistency, which was not observed after sTRAIL administration or injection of CD34-mock cells. Indeed, beyond the pyknotic nuclei resulting from chromatin condensation in apoptotic cells, morphologic examination of hematoxylin and eosin-stained sections revealed areas with reduced hematoxylin stainability and patches of destroyed tissue that were not seen in mock- or sTRAIL-treated animals (Figure 5A). TUNEL staining of tumor sections from untreated, mock-, and sTRAIL-treated mice revealed a homogeneous mass of viable cells with necrotic areas accounting only for 1.4% plus or minus 1.0%, 1.8% plus or minus 1%, and 2.9% plus or minus 1% of total tissue, respectively (Figure 5A-B). In contrast, tumors from CD34-TRAIL–treated mice displayed a significant increase of necrotic areas compared with controls (Figure 5B). After a single intravenous administration of CD34-TRAIL+ cells, the percentages of necrotic areas per tissue section ranged from 6% to 18%, resulting in a mean 8-fold increase over controls (11% ± 3.8% vs 1.4% ± 1.0%, $P < .001$) and a 4-fold increase over sTRAIL-treated mice (11% ± 3.8% vs 2.9% ± 1%, $P < .001$; Figure 5B). Pharmacologic manipulation of intratumor recruitment of CD34-TRAIL+ cells using AMD3100, anti–VCAM-1 antibody, or the combination significantly reduced necrotic areas by 37% ($P = .02$), 56% ($P = .002$), and 48% ($P = .003$), respectively (Figure 5C), suggesting that intratumor recruitment of CD34-TRAIL+ cells specifically triggered tumor necrosis.

Hematoxylin and eosin staining revealed red blood cells infiltrating tumor tissue within necrotic areas, close to damaged vessels (not shown). This finding was a distinctive feature of treatment with CD34-TRAIL+ cells and was further confirmed by immunohistochemical staining with glycophorin A (Figure 5A). Hemorrhagic phenomena exactly matched TUNEL+ areas; and indeed, confocal microscopy of TUNEL-stained sections from CD34-TRAIL–treated mice (Figure 4Axvi) revealed the presence of apoptotic endothelial cells. In striking contrast, apoptotic vessels could not be detected in untreated or sTRAIL-treated tumor tissue (Figure 4Axiii-xv), suggesting that only CD34-TRAIL+ cells could effectively trigger apoptosis of tumor endothelial cells. In addition, no evidence of tissue or vascular damage and hemorrhagic necrosis was detected in healthy tissues, including lung, liver, spleen, and femur, suggesting a tumor-restricted antivascular activity by CD34-TRAIL+ cells (Figure 6).

Antivascular effects of CD34-TRAIL+ cells

To better understand the relationship between the antitumor effects of CD34-TRAIL+ cells and apoptosis of endothelial cells, we performed an extensive vascular analysis on histologic sections from tumor xenografts treated with transduced cells and subsequently biotinylated in vivo. In untreated mice, tumor vasculature was abundant, tortuous, and evenly distributed throughout the tumor, which thus appeared well vascularized (Figure 7A). In

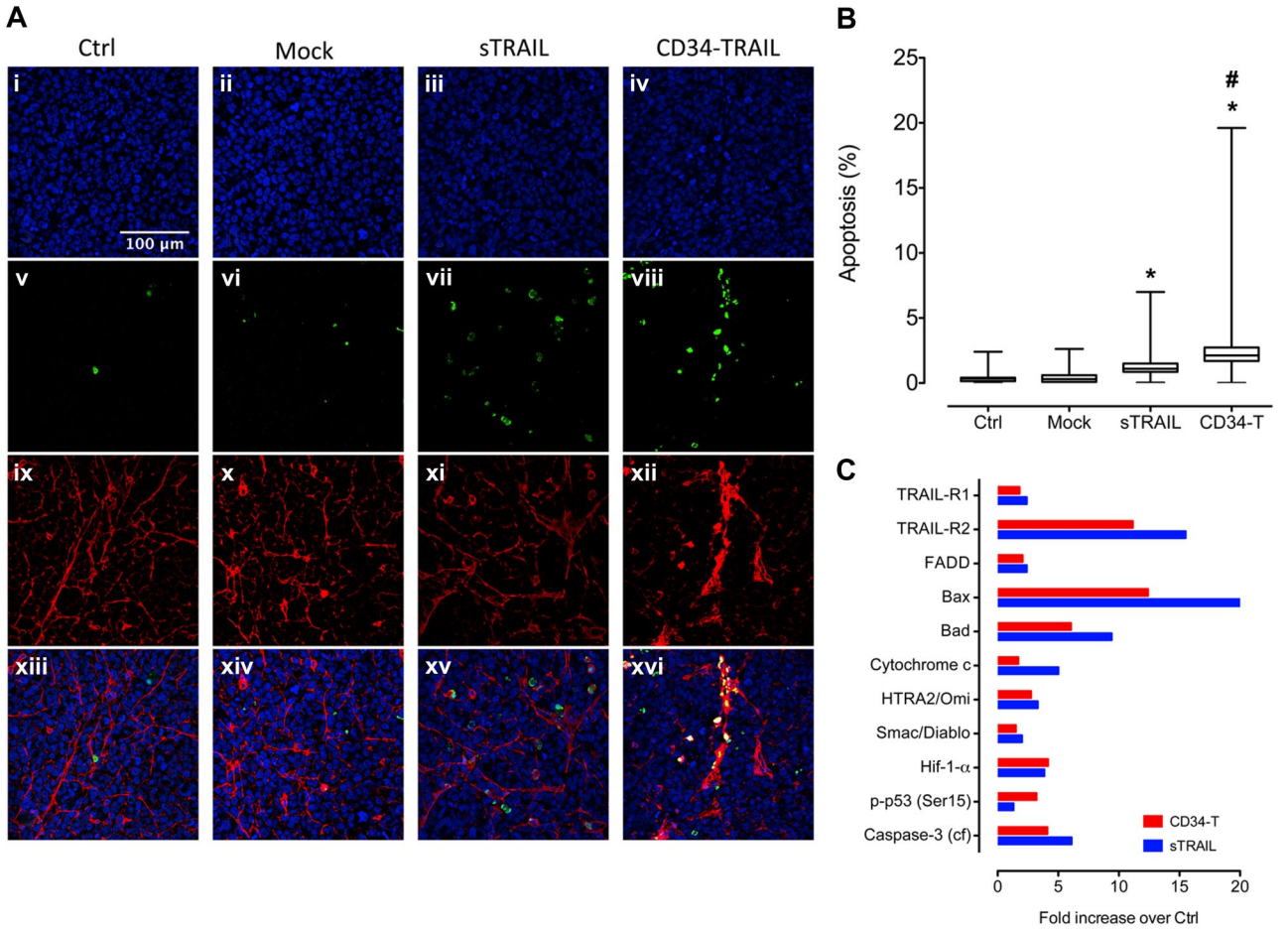

Figure 4. Proapoptotic effects of CD34-TRAIL$^+$ cells. NOD/SCID mice bearing subcutaneous tumor nodules 10 mm in diameter were randomly assigned to receive CD34-TRAIL$^+$ cells, mock-transduced CD34$^+$ cells (3×10^6 cells/mouse, intravenously), recombinant sTRAIL (500 μg/mouse, intraperitoneally), or control vehicle. Forty-eight hours after treatment, NOD/SCID mice were intravenously injected with sulfo-NHS-LC-biotin to biotinylate tumor vasculature. (A) Representative confocal images of tumors from untreated and treated animals processed by triple immunofluorescence staining. (i-iv) Cell nuclei were detected in blue by TO-PRO-3. (v-viii) Apoptotic cells were detected in green by TUNEL staining. (ix-xii) Tumor endothelial cells were detected in red by Alexa 568–conjugated streptavidin. (xiii-xvi) After merging of single-color images, apoptotic nuclei (green) were detectable throughout tumor parenchyma after treatment with either sTRAIL or CD34-TRAIL$^+$ cells, whereas endothelial cells with apoptotic nuclei (yellow) could be detected only in CD34-TRAIL$^+$ cell-treated animals. Objective lens, original magnification: 1.0 NA oil objective, 40×. (B) Percentages of apoptotic cells in tumors from untreated or treated animals were computationally calculated on digitally acquired images (objective lens, original magnification 20×) using ImageJ. At least 3 sections from different animals were analyzed. The boxes extend from the 25th to the 75th percentiles, the lines indicate the median values, and the whiskers indicate the range of values. *$P < .001$, compared with controls. #$P < .001$, compared with sTRAIL. (C) Tissue sections were processed using the Proteome Profiler Human Apoptosis array kit to detect apoptosis-related proteins. Array images were collected on x-ray films and scanned for analysis with ImageJ. Data are shown as fold increase over controls. A representative experiment is shown. cf indicates cleaved fragment.

striking contrast, in NOD/SCID mice treated with CD34-TRAIL$^+$ cells, viable tumor cells surrounding necrotic areas appeared deficient in capillaries and small-caliber blood vessels, which were less tortuous and had fewer branches and sprouts (Figure 7A). Globally, mean percentages of endothelial areas from control and mock-treated tumors were 8.8% plus or minus 5.6% and 8.2% plus or minus 3.3%, respectively (Figure 7B). Administration of sTRAIL did not affect endothelial area compared with controls (8.1% ± 2.9% vs 8.8% ± 5.6%, P = not significant). In contrast, a single intravenous injection of 3×10^6 CD34-TRAIL$^+$ cells caused a 37% decrease of endothelial area compared with control (5.6% ± 3.2% vs 8.8% ± 5.6%, $P < .001$; Figure 7B). In addition, blood vessels from tumors treated with CD34-TRAIL$^+$ cells were thicker than those observed in untreated or sTRAIL-treated animals (Figure 7A). Based on these findings, we isolated images of transversally oriented vessels in streptavidin-HRP-stained sections and calculated vessel wall thickness by processing images with ImageJ and specifically written macros. As shown in Figure 7C, wall thickness was 1.7-fold increased compared with control in vessels surviving the treatment with CD34-TRAIL$^+$ cells (5.5 ± 1.4 μm vs 3.2 ± 0.8 μm, $P < .001$), whereas no increases emerged after sTRAIL administration (3.3 ± 0.7 μm vs 3.2 ± 0.8 μm).

Discussion

We have previously demonstrated that intravenous injection of CD34-TRAIL$^+$ cells in mice with systemic multiple myeloma exerts a marked antitumor activity, resulting in a significant increase of median survival.[29] The present study combined histologic and computer-aided analyses to investigate the antitumor and antivascular activity of mTRAIL-expressing cells. To analyze tumor vasculature, we took advantage of an in vivo assay for endothelial cell staining.[32] Under our experimental conditions, this assay allows an accurate analysis of tumor but not bone marrow vasculature, resulting from a marked extravasation of sulfo-biotin from bone marrow sinusoids. Thus, despite a systemic disease model that should have allowed analysis of multiple myeloma cells in their microenvironment, ie, the bone marrow, we were forced to

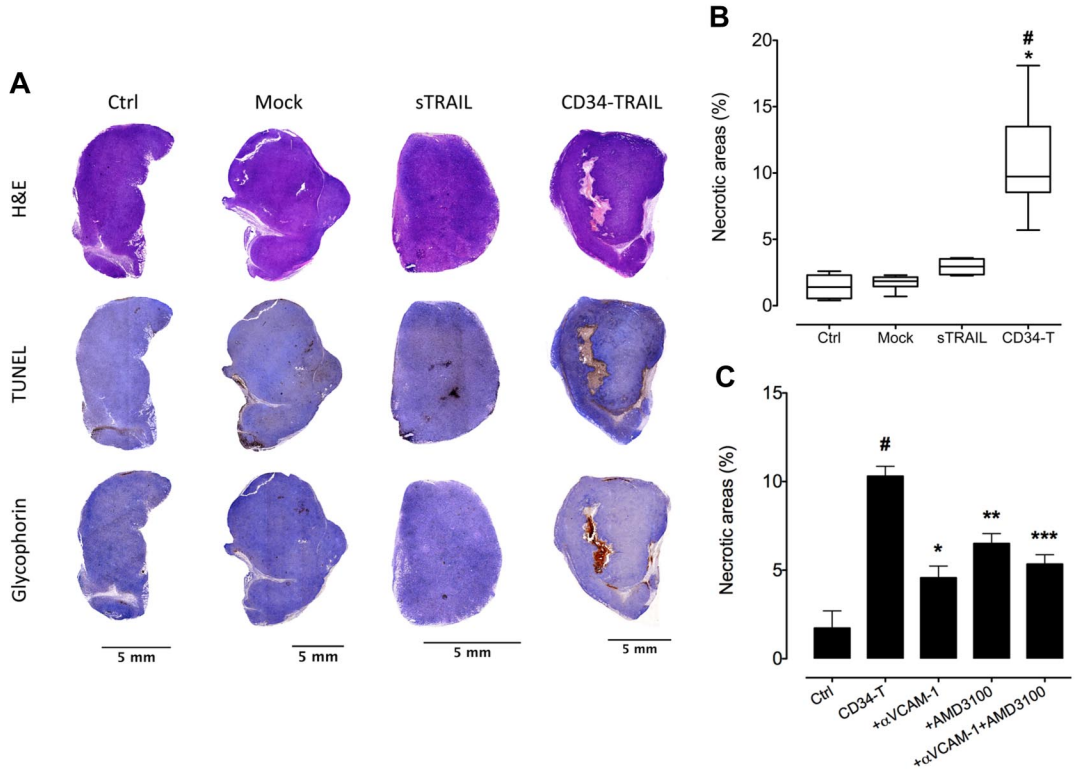

Figure 5. A single injection of CD34-TRAIL+ cells induces tumor necrosis. (A) NOD/SCID mice bearing subcutaneous tumor nodules 10 mm in diameter were randomly assigned to receive CD34-TRAIL+ cells, mock-transduced CD34+ cells (3×10^6 cells/mouse, intravenously), recombinant sTRAIL (500 μg/mouse, intraperitoneally), or control vehicle. Hematoxylin and eosin, TUNEL, and glycophorin A staining was performed. Objective lens, original magnification: 0.08 NA dry objective, 2×. (B) Quantification of necrotic areas by ImageJ analysis on digitally acquired tissue sections stained with TUNEL. At least 6 sections from different animals were analyzed per treatment group. The boxes extend from the 25th to the 75th percentiles, the lines indicate the median values, and the whiskers indicate the range of values. *$P < .001$, compared with controls. #$P < .001$, compared with sTRAIL. (C) Injection of anti–VCAM-1 and AMD3100 reduced tumor necrosis in mice treated with CD34-TRAIL+ cells. Necrotic areas (± SD) were quantified by ImageJ analysis. Data from 1 representative experiment are shown. #$P < .001$, compared with control. *$P = .002$, compared with CD34-TRAIL+ cells. **$P = .02$, compared with CD34-TRAIL+ cells. ***$P = .003$, compared with CD34-TRAIL+ cells.

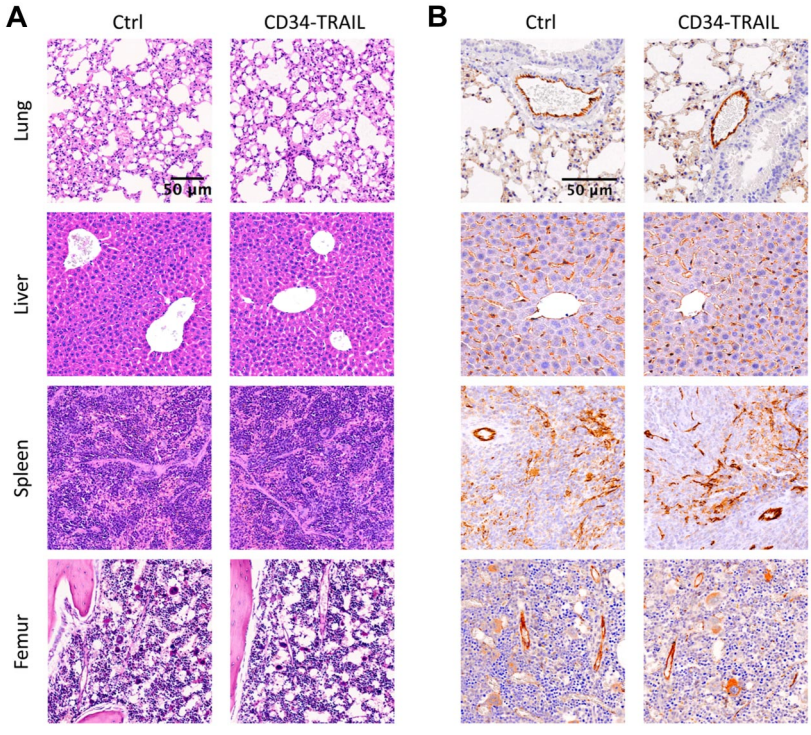

Figure 6. Tissue and vascular toxicity in healthy tissue after CD34-TRAIL+ cell administration. NOD/SCID mice bearing subcutaneous tumor nodules received a single intravenous injection of CD34-TRAIL+ cells (3×10^6 cells/mouse) or control vehicle. Forty-eight hours after treatment, lung, liver, spleen, and femur were harvested and analyzed. (A) Hematoxylin and eosin and (B) immunohistochemical staining with anti-CD31 antibody demonstrated the absence of tissue or vascular damage. Representative histologic images are shown. Objective lens, original magnifications: (A) 0.4 NA dry objective, 10×; (B) 0.75 NA dry objective, 20×.

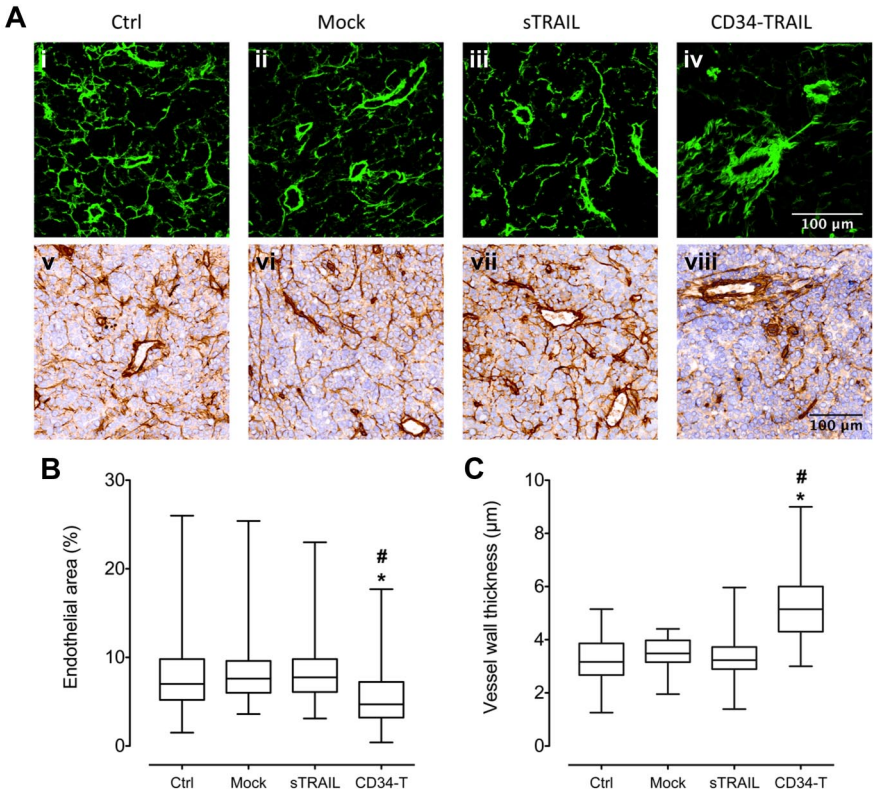

Figure 7. Antivascular effects of CD34-TRAIL$^+$ cells. (A) NOD/SCID mice bearing subcutaneous tumor nodules 10 mm in diameter were randomly assigned to receive CD34-TRAIL$^+$ cells, mock-transduced CD34$^+$ cells (3×10^6 cells/mouse, intravenously), recombinant sTRAIL (500 μg/mouse, intraperitoneally), and control vehicle. Forty-eight hours after treatment, NOD/SCID mice were intravenously injected with 0.2 mL of sulfo-NHS-LC-biotin (5 mg/mL) to biotinylate tumor vasculature. Tumors were then excised, and biotinylated endothelium was revealed by AlexaFluor 488–streptavidin for confocal microscopy analysis (i-iv; 40×/1.0 NA oil objective) or sequentially incubated with HRP-streptavidin and 3,3′-diaminobenzidine for light microscopy analysis (v-viii; 20×/0.75 NA dry objective). After counterstaining with hematoxylin, sections were analyzed using ImageJ for quantification of vascular parameters. Representative confocal and histologic images of in vivo biotinylated mice receiving the different treatments are shown. (B) Endothelial area was calculated on whole tissue sections as (streptavidin-HRP stained area)/(total tissue area) × 100. *$P < .001$, compared with controls. #$P < .001$, compared with sTRAIL. (C) Vessel wall thickness was calculated on transversally oriented vessels. *$P < .001$, compared with controls. #$P < .001$, compared with sTRAIL.

use a subcutaneous tumor model allowing accurate analysis of tumor vasculature. Our results demonstrate that TRAIL-expressing CD34$^+$ cells can efficiently vehiculate mTRAIL within the tumors where they exert a potent antivascular and antitumor activity. In addition, repeated administration of CD34-TRAIL$^+$ cells significantly slowed the growth of subcutaneous KMS-11 xenografts and significantly reduced tumor volumes.

Kinetics data clearly show that intravenously injected transduced cells circulate in normal tissues up to 24 hours, but they progressively and preferentially home at tumor sites where they can be detected up to 48 hours after injection. Lack of intratumor detection of CD34-TRAIL$^+$ cells beyond 48 hours after injection (data not shown) may be the result of destruction of mTRAIL-expressing cells in the context of antitumor activities (eg, disruption of tumor vasculature, hemorrhagic necrosis, and tumor necrosis).

Increasing evidence suggests that recruitment of CD34$^+$ cells in the tumor microenvironment is the result of homing signals similar to those found in the bone marrow hematopoietic niches.[4,6,7,39] Both SDF-1/CXCR4 and VCAM-1/VLA-4 pathways play a key role in regulating bone marrow homing of transplanted hematopoietic stem cells[37,40] as well as intratumor recruitment of CXCR4-expressing cells and neovascularization during acute ischemia and tumor growth.[3,4,41] Tumor homing of CD34-TRAIL$^+$ cells involves a variety of regulatory mechanisms, including SDF-1/CXCR4 and VCAM-1/VLA-4. Pharmacologic manipulation of adhesion receptor expression using either AMD3100 or anti–VCAM-1 antibodies significantly reduced both the frequency and the antitumor efficacy of CD34-TRAIL$^+$ cells, strongly suggesting that SDF-1 and VCAM-1 expressed by tumor vasculature efficiently recruit transduced CD34$^+$ cells within tumors by challenging their trafficking and homing properties. The role of additional binding systems, such as mTRAIL/TRAIL-R2, in mediating tumor tropism of CD34-TRAIL$^+$ cells may be hypothesized on the basis of data reported herein but is not formally demonstrated in this study and will require further experiments. Indeed, binding of CD34-TRAIL$^+$ cells to TRAIL-R2 expressed by tumor vasculature could significantly contribute to initiation of a cascade of events that induce early endothelial damage, leading to extensive tumor cell death.[42] Further experiments are currently ongoing to identify critical molecular mediators of the vascular-disrupting activity of mTRAIL.

In addition to a significant tumor growth delay that was even increased compared with that induced by sTRAIL, CD34-TRAIL$^+$ cells induced objectively measurable changes in subcutaneous tumor nodules. First, TUNEL staining and protein array profiling of tumor nodules obtained 48 hours after a single administration of transduced cells showed that TRAIL-expressing cells were 2-fold more effective than sTRAIL in inducing apoptosis of tumor cells while activating a similar cell death machinery. Second, conspicuous and broad necrotic events, involving up to 18% of tumor tissue, were detected only after administration of CD34-TRAIL$^+$ cells. Third, these necrotic events were associated with a hemorrhagic component, as shown by antiglycophorin-mediated labeling of red blood cells infiltrating tumor parenchyma, which was not detectable after sTRAIL administration. Finally, hemorrhagic necrosis was localized near TUNEL$^+$ blood vessels, suggesting that apoptosis of tumor endothelial cells represents an early event triggered by CD34-TRAIL$^+$ cells. Overall, these findings support the hypothesis that CD34-TRAIL$^+$ cells exert their cytotoxic activity not only by targeting parenchymal tumor cells but also by targeting tumor vasculature.[29] The vascular-disrupting activity of mTRAIL might represent a major concern in view of clinical applications. Notwithstanding the intratumor vascular-disrupting activity of mTRAIL, extensive analysis of healthy tissues failed to detect any evidence of hemorrhagic necrosis, strongly suggesting that vascular damage was tumor-restricted.

Streptavidin-mediated in vivo identification of tumor vessels allowed an efficient labeling of functional (ie, perfused) tumor vasculature, regardless of vessel size and limitations related to cell-surface antigen expression and retrieval.[43] When combined with TUNEL staining, endothelium biotinylation allowed a virtually objective quantification of tissue damage involving both tumor cells and tumor vasculature. Indeed, the use of ImageJ and specifically written macros allowed analysis of entire tumor sections, avoiding the need for manual selection of representative fields. Interobserver variation in recognition and counting of parameters was thus greatly reduced by this semiautomated image analysis that allowed interactive correction when required but that overall avoided the manual selection of "hot spots."[43]

Treatment with CD34-TRAIL$^+$ cells induced a significant reduction of tumor endothelial cells, a marked fragmentation of surviving vessels, and an increased thickness of vessel walls, a plausible sign of cytoskeletal endothelial cell reorganization.[44] Such a marked and tumor selective vascular damage exerted by as low as 0.2% tumor-infiltrating CD34-TRAIL$^+$ cells will require further investigation.[45,46] Tumor vessels are expected to have a higher sensitivity to cytotoxic agents than normal endothelial cells. In contrast to their normal counterparts, tumor endothelial cells are characterized by loosening of adhesion to surrounding cells (including pericytes) and to the extracellular matrix, increased permeability resulting from widening of intercellular junctions, a discontinuous basement membrane, and transcellular holes, vesicles, and fenestrae.[47]

In conclusion, under our experimental conditions, the use of transduced CD34$^+$ cells as a vehicle of mTRAIL resulted in an antitumor effect greater than that exerted by sTRAIL, probably because of an antivascular action. Our findings appear to be of outstanding interest in the context of the increasing need for therapeutic strategies targeting not only tumor cells but also the tumor microenvironment.[7,36,48] Furthermore, the ability of CD34-TRAIL$^+$ cells to home within and distribute through tumor masses could induce more complete, tumor-driven, antitumor responses compared with agents with more restricted distribution potential, such as modified liposomes, conjugated antibodies, nanoparticles, or polymers, modified viruses of various genotypes, or tumor/organ-specific expression cassettes.[11,49] Finally, the clinical feasibility of such a systemic CD34$^+$ cell-based gene therapy approach could be exploited to develop effective autologous or allogeneic anticancer treatments.

Acknowledgments

This work was supported in part by Ministero dell'Istruzione, dell'Università e della Ricerca (Rome, Italy), Ministero della Salute (Rome, Italy), Alleanza Contro il Cancro (Rome, Italy), and the Michelangelo Foundation for Advances in Cancer Research and Treatment (Milano, Italy).

Authorship

Contribution: C.L. performed experiments, collected and interpreted data, and wrote the manuscript; C.C.-S. designed research, analyzed and interpreted data, performed statistical analysis, and wrote the manuscript; A. Giacomini performed experiments and collected, analyzed, and interpreted data; L.C. performed experiments and collected data; M.R. performed image analysis and analyzed and interpreted data; D.S., P.L., M. Milanesi, and M.F. performed experiments; M.D.N. analyzed and interpreted data; M. Magni performed experiments and analyzed and interpreted data; A. Gloghini, A.C., and F.F. analyzed and interpreted data; and A.M.G. designed research, analyzed and interpreted data, and approved the manuscript.

Conflict-of-interest disclosure: The authors declare no competing financial interests.

Correspondence: Carmelo Carlo-Stella, Cristina Gandini Medical Oncology Unit, Fondazione Istituto di Ricovero e Cura a Carattere Scientifico Istituto Nazionale Tumori, Via Venezian, 1-20133 Milano, Italy; e-mail: carmelo.carlostella@unimi.it.

References

1. Harrington K, Alvarez-Vallina L, Crittenden M, et al. Cells as vehicles for cancer gene therapy: the missing link between targeted vectors and systemic delivery? *Hum Gene Ther.* 2002;13(11):1263-1280.
2. Introna M, Barbui AM, Golay J, Rambaldi A. Innovative cell-based therapies in onco-hematology: what are the clinical facts? *Haematologica.* 2004;89(10):1253-1260.
3. Burger JA, Kipps TJ. CXCR4: a key receptor in the crosstalk between tumor cells and their microenvironment. *Blood.* 2006;107(5):1761-1767.
4. Jin H, Aiyer A, Su J, et al. A homing mechanism for bone marrow-derived progenitor cell recruitment to the neovasculature. *J Clin Invest.* 2006;116(3):652-662.
5. Kucia M, Reca R, Miekus K, et al. Trafficking of normal stem cells and metastasis of cancer stem cells involve similar mechanisms: pivotal role of the SDF-1-CXCR4 axis. *Stem Cells.* 2005;23(7):879-894.
6. Kaplan RN, Psaila B, Lyden D. Niche-to-niche migration of bone-marrow-derived cells. *Trends Mol Med.* 2007;13(2):72-81.
7. Rafii S, Lyden D, Benezra R, Hattori K, Heissig B. Vascular and haematopoietic stem cells: novel targets for anti-angiogenesis therapy? *Nat Rev Cancer.* 2002;2(11):826-835.
8. Najbauer J, Danks M, Schmidt N, Kim S, Aboody K. Neural stem cell-mediated therapy of primary and metastatic solid tumors. Progress in Gene Therapy, Autologous and Cancer Stem Cell Gene Therapy World Scientific: Singapore, 2007.
9. Loebinger MR, Eddaoudi A, Davies D, Janes SM. Mesenchymal stem cell delivery of TRAIL can eliminate metastatic cancer. *Cancer Res.* 2009;69(10):4134-4142.
10. Aboody KS, Najbauer J, Danks MK. Stem and progenitor cell-mediated tumor selective gene therapy. *Gene Ther.* 2008;15(10):739-752.
11. Griffith TS, Stokes B, Kucaba TA, et al. TRAIL gene therapy: from preclinical development to clinical application. *Curr Gene Ther.* 2009;9(1):9-19.
12. Sasportas LS, Kasmieh R, Wakimoto H, et al. Assessment of therapeutic efficacy and fate of engineered human mesenchymal stem cells for cancer therapy. *Proc Natl Acad Sci U S A.* 2009;106(12):4822-4827.
13. Ashkenazi A, Pai RC, Fong S, et al. Safety and antitumor activity of recombinant soluble Apo2 ligand. *J Clin Invest.* 1999;104(2):155-162.
14. Gazitt Y. TRAIL is a potent inducer of apoptosis in myeloma cells derived from multiple myeloma patients and is not cytotoxic to hematopoietic stem cells. *Leukemia.* 1999;13(11):1817-1824.
15. Pollack IF, Erff M, Ashkenazi A. Direct stimulation of apoptotic signaling by soluble Apo2L/tumor necrosis factor-related apoptosis-inducing ligand leads to selective killing of glioma cells. *Clin Cancer Res.* 2001;7(5):1362-1369.
16. Jin H, Yang R, Fong S, et al. Apo2 ligand/tumor necrosis factor-related apoptosis-inducing ligand cooperates with chemotherapy to inhibit orthotopic lung tumor growth and improve survival. *Cancer Res.* 2004;64(14):4900-4905.
17. Mitsiades CS, Treon SP, Mitsiades N, et al. TRAIL/Apo2L ligand selectively induces apoptosis and overcomes drug resistance in multiple myeloma: therapeutic applications. *Blood.* 2001;98(3):795-804.
18. Rieger J, Naumann U, Glaser T, Ashkenazi A, Weller M. APO2 ligand: a novel lethal weapon against malignant glioma? *FEBS Lett.* 1998;427(1):124-128.
19. Daniel D, Yang B, Lawrence DA, et al. Cooperation of the proapoptotic receptor agonist rhApo2L/TRAIL with the CD20 antibody rituximab against non-Hodgkin lymphoma xenografts. *Blood.* 2007;110(12):4037-4046.
20. Kelley SK, Harris LA, Xie D, et al. Preclinical studies to predict the disposition of Apo2L/tumor necrosis factor-related apoptosis-inducing ligand in humans: characterization of in vivo efficacy, pharmacokinetics, and safety. *J Pharmacol Exp Ther.* 2001;299(1):31-38.

21. Ashkenazi A, Holland P, Eckhardt SG. Ligand-based targeting of apoptosis in cancer: the potential of recombinant human apoptosis ligand 2/tumor necrosis factor-related apoptosis-inducing ligand (rhApo2L/TRAIL). *J Clin Oncol.* 2008;26(21):3621-3630.
22. Walczak H, Miller RE, Ariail K, et al. Tumoricidal activity of tumor necrosis factor-related apoptosis-inducing ligand in vivo. *Nat Med.* 1999; 5(2):157-163.
23. Ballestrero A, Nencioni A, Boy D, et al. Tumor necrosis factor-related apoptosis-inducing ligand cooperates with anticancer drugs to overcome chemoresistance in antiapoptotic Bcl-2 family members expressing Jurkat cells. *Clin Cancer Res.* 2004;10(4):1463-1470.
24. Inoue S, Macfarlane M, Harper N, Wheat LM, Dyer MJ, Cohen GM. Histone deacetylase inhibitors potentiate TNF-related apoptosis-inducing ligand (TRAIL)-induced apoptosis in lymphoid malignancies. *Cell Death Differ.* 2004;11[suppl 2]:S193-S206.
25. Kim SM, Lim JY, Park SI, et al. Gene therapy using TRAIL-secreting human umbilical cord blood-derived mesenchymal stem cells against intracranial glioma. *Cancer Res.* 2008;68(23):9614-9623.
26. Mohr A, Lyons M, Deedigan L, et al. Mesenchymal stem cells expressing TRAIL lead to tumour growth inhibition in an experimental lung cancer model. *J Cell Mol Med.* 2008;12(6):2628-2643.
27. Uzzaman M, Keller G, Germano IM. In vivo gene delivery by embryonic-stem-cell-derived astrocytes for malignant gliomas. *Neuro Oncol.* 2009; 11(2):102-108.
28. Menon LG, Kelly K, Wei Yang H, Kim SK, Black PM, Carroll RS. Human bone marrow derived mesenchymal stromal cells expressing S-TRAIL as a cellular delivery vehicle for human glioma therapy. *Stem Cells.* 2009;27(9):2320-2330.
29. Carlo-Stella C, Lavazza C, Di Nicola M, et al. Antitumor activity of human CD34(+) cells expressing membrane-bound tumor necrosis factor-related apoptosis-inducing ligand. *Hum Gene Ther.* 2006;17:1225-1240.
30. Carlo-Stella C, Lavazza C, Locatelli A, Vigano L, Gianni AM, Gianni L. Targeting TRAIL agonistic receptors for cancer therapy. *Clin Cancer Res.* 2007;13(8):2313-2317.
31. Carlo-Stella C, Lavazza C, Carbone A, Gianni AM. Anticancer cell therapy with TRAIL-armed CD34+ progenitor cells. *Adv Exp Med Biol.* 2008; 610:100-111.
32. Rybak JN, Ettorre A, Kaissling B, Giavazzi R, Neri D, Elia G. In vivo protein biotinylation for identification of organ-specific antigens accessible from the vasculature. *Nat Methods.* 2005;2(4):291-298.
33. Broxmeyer HE. Chemokines in hematopoiesis. *Curr Opin Hematol.* 2008;15(1):49-58.
34. Kayagaki N, Yamaguchi N, Nakayama M, et al. Involvement of TNF-related apoptosis-inducing ligand in human CD4+ T cell-mediated cytotoxicity. *J Immunol.* 1999;162(5):2639-2647.
35. Lavazza C, Carlo-Stella C, Di Nicola M, et al. Highly efficient gene transfer into mobilized CD34+ hematopoietic cells using serotype-5 adenoviral vectors and BoosterExpress Reagent. *Exp Hematol.* 2007;35(6):888-897.
36. De Raeve H, Van Marck E, Van Camp B, Vanderkerken K. Angiogenesis and the role of bone marrow endothelial cells in haematological malignancies. *Histol Histopathol.* 2004;19(3):935-950.
37. Peled A, Petit I, Kollet O, et al. Dependence of human stem cell engraftment and repopulation of NOD/SCID mice on CXCR4. *Science.* 1999; 283(5403):845-848.
38. Fricker SP, Anastassov V, Cox J, et al. Characterization of the molecular pharmacology of AMD3100: a specific antagonist of the G-protein coupled chemokine receptor, CXCR4. *Biochem Pharmacol.* 2006;72(5):588-596.
39. Wels J, Kaplan RN, Rafii S, Lyden D. Migratory neighbors and distant invaders: tumor-associated niche cells. *Genes Dev.* 2008;22(5):559-574.
40. Aiuti A, Webb IJ, Bleul C, Springer T, Gutierrez-Ramos JC. The chemokine SDF-1 is a chemoattractant for human CD34+ hematopoietic progenitor cells and provides a new mechanism to explain the mobilization of CD34+ progenitors to peripheral blood. *J Exp Med.* 1997;185(1):111-120.
41. Petit I, Jin D, Rafii S. The SDF-1-CXCR4 signaling pathway: a molecular hub modulating neoangiogenesis. *Trends Immunol.* 2007;28(7):299-307.
42. Arafat WO, Casado E, Wang M, et al. Genetically modified CD34+ cells exert a cytotoxic bystander effect on human endothelial and cancer cells. *Clin Cancer Res.* 2000;6(11):4442-4448.
43. Vermeulen PB, Gasparini G, Fox SB, et al. Second international consensus on the methodology and criteria of evaluation of angiogenesis quantification in solid human tumours. *Eur J Cancer.* 2002;38(12):1564-1579.
44. Tozer GM, Prise VE, Wilson J, et al. Mechanisms associated with tumor vascular shut-down induced by combretastatin A-4 phosphate: intravital microscopy and measurement of vascular permeability. *Cancer Res.* 2001;61(17):6413-6422.
45. Zauli G, Secchiero P. The role of the TRAIL/TRAIL receptors system in hematopoiesis and endothelial cell biology. *Cytokine Growth Factor Rev.* 2006;17(4):245-257.
46. Cao L, Du P, Jiang SH, Jin GH, Huang QL, Hua ZC. Enhancement of antitumor properties of TRAIL by targeted delivery to the tumor neovasculature. *Mol Cancer Ther.* 2008;7(4):851-861.
47. Vacca A, Ria R, Semeraro F, et al. Endothelial cells in the bone marrow of patients with multiple myeloma. *Blood.* 2003;102(9):3340-3348.
48. Joyce JA. Therapeutic targeting of the tumor microenvironment. *Cancer Cell.* 2005;7(6):513-520.
49. Waehler R, Russell SJ, Curiel DT. Engineering targeted viral vectors for gene therapy. *Nat Rev Genet.* 2007;8(8):573-587.